Corresponding author:
Jerry Z. X. Lei;
Email: jerrylei@uvic.ca

Morphological trends across the Norian/Rhaetian boundary within Late Triassic conodonts in western Canada: implications for protracted paleoenvironmental disturbance preceding the end-Triassic mass extinction

Jerry Z. X. Lei[1] (ID), Martyn L. Golding[2] and Jon M. Husson[1]

[1]School of Earth and Ocean Sciences, University of Victoria, Victoria, British Columbia V8P 5C2, Canada
[2]Geological Survey of Canada, Pacific–Vancouver, Vancouver, British Columbia V6B 5J3, Canada

Non-technical Summary

Conodonts were marine vertebrates with tooth-like structures that are commonly preserved in the fossil record. The Late Triassic conodont species *Mockina* ex gr. *carinata* and *Mockina* ex gr. *englandi* were exceptionally prevalent among marine animals from the middle Norian through to the Rhaetian stages of geologic time. Leading into the complete extinction of conodonts near the Triassic/Jurassic boundary, a significant change in conodont forms occurred across the Norian/Rhaetian boundary (NRB), with the common Rhaetian varieties from Europe exhibiting thinner shapes. This trend is not as evident in North America, where these varieties are very rare, but analyses on *M.* ex gr. *carinata* and *M.* ex gr. *englandi* specimens from across western Canadian demonstrate that comparable shifts in form occurred in North America across the NRB, confirming the global extent of these trends. The specimens of *M.* ex gr. *carinata* display a sequential width reduction from the middle Norian to late Norian to Rhaetian, whereas the specimens of *M.* ex gr. *englandi* display a width reduction only from the late Norian to Rhaetian. Specimens of both species that have a length to mid-breadth ratio greater than 3:1 are restricted to the Rhaetian. Specimens from the Kennecott Point section on Haida Gwaii, British Columbia, demonstrate that this shift in form occurred somewhat later than other events and changes associated with the NRB. The global trend of width reduction in many conodonts may reflect a change in diet away from hard food sources, perhaps suggesting some degree of pressure on the biological precipitation of minerals beginning around the NRB. This interpretation would support CO_2 release as the causal mechanism of the environmental disturbance at the NRB and identify the NRB as a significant turning point for Late Triassic ecosystems, marking the beginning of a protracted, multiphase end-Triassic mass extinction.

Abstract

The Late Triassic conodont species *Mockina* ex gr. *carinata* and *Mockina* ex gr. *englandi* were exceptionally prevalent among the marine fauna of the Panthalassan realm from the middle Norian through to the Rhaetian. Leading into the complete extinction of conodonts near the Triassic/Jurassic boundary, a significant turnover event occurred in conodont fauna across the Norian/Rhaetian boundary (NRB), with the pectiniform elements of common Rhaetian genera from Tethys exhibiting minimal or absent platforms. This intergeneric trend of platform reduction is not as evident in Panthalassa, where these genera are very rare, but morphometric analyses of *M.* ex gr. *carinata* and *M.* ex gr. *englandi* specimens from across the Canadian Cordillera demonstrate that comparable shifts in morphology occurred intraspecifically in Panthalassa across the NRB, confirming the global extent of these trends. Pectiniform elements of *M.* ex gr. *carinata* display a sequential reduction of platform width from the middle Norian to late Norian to Rhaetian, whereas pectiniform elements of *M.* ex gr. *englandi* display a reduction of platform width only from the late Norian to Rhaetian. Specimens of both species that have a mid-platform length to breadth ratio greater than 3:1 are restricted to the Rhaetian. Specimens from the Kennecott Point section on Haida Gwaii, British Columbia, demonstrate that this morphological shift occurred somewhat later than other biostratigraphic proxies for the NRB. The global trend of platform width reduction in many conodont pectiniform elements may reflect a change in primary diet away from hard food sources, perhaps suggesting some degree of carbonate biomineralization suppression beginning around the NRB. This interpretation would support CO_2 outgassing as the causal mechanism of the environmental disturbance at the NRB and identify the NRB as a significant turning point for Late Triassic ecosystems, marking the beginning of a protracted, multiphase end-Triassic mass extinction.

Introduction

The Middle to Late Triassic was a unique time in geologic history in which "modern fauna" was first able to extensively radiate and thrive following the drawn-out aftermath of the Permian/Triassic mass extinction (e.g., Sepkoski 1981; Raup and Sepkoski 1982). During this interval, the global biosphere experienced a short-lived diversity peak in the Late Triassic, before being devastated by the subsequent end-Triassic mass extinction (ETME) (e.g., Sepkoski 1981; Raup and Sepkoski 1982). Much emphasis has been placed on investigating both of these mass extinctions, but research on the broader paleobiologic trends across the Late Triassic has been much less common. Mass extinction events are traditionally thought of as geologically instantaneous, but there is considerable evidence that the paleoenvironmental disturbance and biotic distress associated with the ETME began before the actual Triassic/Jurassic boundary (e.g., Hesselbo et al. 2002; Ward et al. 2004; Ruhl and Kürschner 2011; Schoepfer et al. 2016; Davies et al. 2017; Yager et al. 2017; Larina et al. 2019). Some have even argued that the ETME may be better characterized as the aggregation of multiple temporally disparate biotic turnover events throughout the latest Triassic, beginning as early as the Norian/Rhaetian boundary (NRB) (e.g., Hallam 2002; Tanner et al. 2004; Lucas 2018; Rigo et al. 2018, 2020). Many faunal groups experienced significant turnover at the NRB, including bivalves, conodonts, radiolarians, and ammonoids (e.g., Ward et al. 2001, 2004; Tanner et al. 2004; Carter and Orchard 2007; Lucas 2018; Rigo et al. 2018, 2020). Recovery within these faunal groups was limited during the Rhaetian, potentially suggesting a prolonged interval of elevated environmental stress persisting after the NRB, which in turn contributed to the severity of the ETME, because a fragile biosphere would be more vulnerable to extinction pressures (e.g., Hallam 2002; Tanner et al. 2004; Lucas 2018; Rigo et al. 2018, 2020). For example, although coral reefs are present in Rhaetian strata, they are considerably smaller in size and less widespread compared with their Norian counterparts, with the latter representing peak diversity in the Triassic (e.g., Flügel and Kiessling 2002; Stanley 2003; Rigo et al. 2020). It was these relatively less robust Rhaetian communities that were then subsequently devastated during the ETME (e.g., Flügel and Kiessling 2002; Stanley 2003; Rigo et al. 2020).

While the primary trigger of the ETME has been broadly accepted as enhanced volcanic outgassing associated with the Central Atlantic Magmatic Province (CAMP) (Marzoli et al. 1999, 2004; Blackburn et al. 2013), the causal mechanism for disturbance at the NRB has remained elusive. A potential mechanism is volcanism preceding CAMP emplacement (e.g., Zaffani et al. 2017; Rigo et al. 2020). This hypothesis is supported indirectly by decreasing $^{87}Sr/^{86}Sr$ ratios in seawater across the NRB, interpreted as an increase in weathering input of mantle-derived volcanics (Korte et al. 2003; Callegaro et al. 2012; Tackett et al. 2014). However, this signal from the Tethyan realm (marine environment on the eastern margin of Pangea) has not been convincingly documented in the Panthalassan realm (marine environment on the western margin of Pangea), arguably undermining its supposed global extent (Lei et al. 2022). Emplacement of the Angayucham Province in Alaska has been proposed as the source of this hypothetical volcanism at the NRB (Zaffani et al. 2017; Rigo et al. 2020), but the poor precision of current age constraints (Ernst and Buchan 2001) makes this link tenuous. The true driver of the NRB disturbance and faunal turnover therefore remains uncertain.

The ETME has long been held to mark the total extinction of the long-ranging class Conodonta (e.g., Clark 1983), with perhaps just a handful of examples globally where rare conodont specimens are found in the earliest Hettangian (Pálfy et al. 2007; Du et al. 2020b, 2023; Caruthers et al. 2022). A general trend of declining conodont diversity is observed throughout the Late Triassic, indicating that the final extinction of the class may be better interpreted as the culmination of a multi-million-year process of deterioration rather than solely as the result of a sudden cataclysmic event (Martínez-Pérez et al. 2014a; Rigo et al. 2018). The latest Norian represents the last significant peak of conodont standing diversity, which then dropped precipitously across the Rhaetian Stage (Martínez-Pérez et al. 2014a; Rigo et al. 2018). This diversity trend points toward the NRB as being a crucially important interval in conodont evolutionary history, the study of which could lead to a better understanding of the ETME and paleoenvironmental conditions preceding it. This in turn may help in determining why the class went extinct during the ETME, after having survived the more severe Permian/Triassic mass extinction (e.g., Sepkoski 1981; Raup and Sepkoski 1982).

Conodont pectiniform element morphology displays a general trend of simplification across the NRB, with the forms of genera like *Misikella* and *Parvigondolella*, which dominate Rhaetian fauna, having minimal platforms or none at all (e.g., Orchard et al. 2007; Giordano et al. 2010; Mazza et al. 2012; Rigo et al. 2018; Karádi et al. 2020; Du et al. 2021, 2023). This is in contrast to the forms that dominate Norian fauna, such as the genera *Epigondolella* and *Mockina*, both of which commonly display prominent platforms hosting sharp and discrete platform denticles; another Norian example is the genus *Norigondolella*, which displays forms with prominent and anteriorly extended platforms, typically resulting in the absence of any free blade (e.g., Orchard 1991a,b, 2018; Mazza et al. 2012; Rigo et al. 2018; Du et al. 2021). The genus *Misikella* is commonly found in the Rhaetian of Tethys, but is extremely rare in the Rhaetian of Panthalassa, such that it has limited biostratigraphic utility in the latter region (Carter and Orchard 2007; Orchard et al. 2007). Comparable trends of platform reduction within pectiniform elements across the NRB interval can potentially still be observed in the morphologies of genera and species that are more abundant in Panthalassa, such as within *Mockina mosheri*. Morphotype B of this species ranges from the latest Norian through Rhaetian, in contrast with morphotypes A and C, which are exclusively Rhaetian (Orchard 1994; Carter and Orchard 2007; Orchard et al. 2007). Morphotype B is unique in possessing accessory platform denticles, resulting in wider platforms overall compared with the exclusively Rhaetian forms (Orchard 1994; Carter and Orchard 2007; Orchard et al. 2007). However, any platform reduction exhibited by *M. mosheri* is considerably less clear than the intergeneric Tethyan trends, as the stratigraphic ranges of all three morphotypes are nearly identical, with morphotype B only differing from the others by extending slightly earlier into the latest Norian. Also, *M. mosheri* may not be the most representative species of Panthalassan fauna, as none of the morphotypes are particularly common in either the Norian or the Rhaetian.

The present study aims to investigate morphological shifts displayed by *Mockina* ex gr. *carinata* and *Mockina* ex gr. *englandi* as these conodont species cross the NRB. Pectiniform elements of these two conodont species have been recovered in exceptionally high abundance from North American strata (Panthalassan realm) ranging from the middle Norian through Rhaetian. Therefore, they make excellent candidates for the application of

morphometric analysis to investigate trends in Panthalassan conodont pectiniform morphology across the NRB interval. No prior morphometric studies have been conducted on these two conodont species or on any conodont species crossing the NRB. If the intergeneric trends of pectiniform platform reduction largely observed in Tethys can also be recognized intraspecifically in species that dominate Panthalassa, this would greatly reinforce the hypothesis that these morphological shifts occurred in response to global-scale stressors.

Materials and Methods

The present study utilizes new and archival collections of *Mockina* ex gr. *carinata* and *Mockina* ex gr. *englandi* from across the Canadian Cordillera (Fig. 1). Limestone samples were processed for conodonts at the Geological Survey of Canada Pacific Division in Vancouver, British Columbia, using standard techniques as outlined by Stone (1987). Individual samples were crushed into ~3 cm fragments before being dissolved in acetic acid for 10–14 days. Per ~1 kg of sample, a solution of 6.0 liters of water, 3.2 liters of 10–15% acetic acid (to create a buffer), and 0.8–1.0 liter of 99.5% glacial acetic acid was used. The residues that remained after treatment were then sieved to collect the 90–850 µm fraction. The isolated fraction was rinsed, dried, and put through heavy-liquid separation using sodium polytungstate (specific gravity of 2.85 kg/L), with the heavy fraction collected.

As the Canadian Cordillera comprises a multitude of allochthonous terranes (e.g., Monger and Ross 1971; Jones et al. 1977; Mihalynuk et al. 1994; Belasky et al. 2002; Johnston and Borel 2007; Johnston 2008; Colpron and Nelson 2009, 2011; Kent and Irving 2010; Beranek and Mortensen 2011), this sampling of specimens represents a wide paleogeographic distribution stretching from the western margin of Laurentia to the open Panthalassic Ocean during the Late Triassic (Fig. 1). Specimen counts classified by terrane affinity and age are summarized in Table 1, and a detailed list of samples can be found in the Supplementary Appendix. Particularly productive localities include the Black Bear Ridge section at

Table 1. Specimen counts of *Mockina carinata* and *Mockina englandi* grouped by terrane affinity and age.

Terrane	Age	*Mockina* ex gr. *carinata*	*Mockina* ex gr. *englandi*
Laurentian margin	Middle Norian	5	0
Laurentian margin	Late Norian	24	69
Laurentian margin	Rhaetian	4	1
Stikine	Middle Norian	15	6
Stikine	Late Norian	61	173
Stikine	Rhaetian	2	2
Wrangell	Middle Norian	11	9
Wrangell	Late Norian	9	24
Wrangell	Rhaetian	23	55

Williston Lake representing the Laurentian margin, the Sinwa East section on Mount Sinwa representing the Stikine Terrane imminently converging with Laurentia, and the Kennecott Point section on Haida Gwaii representing the Wrangell Terrane in open ocean (e.g., Colpron and Nelson 2009, 2011; Fig. 1).

Both *M.* ex gr. *carinata* and *M.* ex gr. *englandi* have previously been included in the genus *Epigondolella*, under a more expansive interpretation of that genus diagnosed by tall and discrete anterior platform denticles (e.g., Orchard 1991b; Carter and Orchard 2007; Orchard et al. 2007). More recent studies have generally reinterpreted these two species as belonging to the genus *Mockina* (e.g., Mazza et al. 2012; Orchard 2018; Du et al. 2020a; Caruthers et al. 2022; Lei et al. 2022). *Mockina* was initially proposed as a derivative of *Epigondolella* in which the bifurcated keel was lost entirely, resulting in a keel that terminates posteriorly in a single point (Kozur 1989a,b). Current differentiation between these two genera also emphasizes the less-ornamented platforms of *Mockina* relative to those of *Epigondolella* (e.g., Mazza et al. 2012; Orchard 2018; Du et al. 2020a). Orchard (1991b) initially defined *M. carinata* as a short species of *Epigondolella* with two large denticles on one anterior platform margin and one large denticle on the other (Fig. 2A). Additional smaller platform denticles continue posteriorly of the large main set (Orchard 1991b). Orchard (1991b) defined the species *M. englandi* similarly,
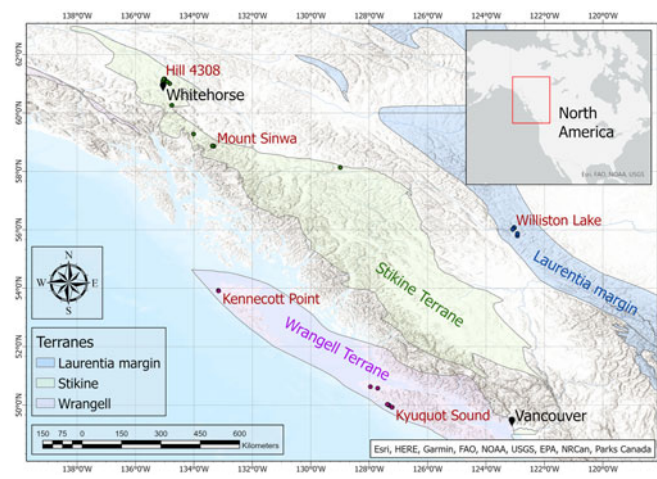

Figure 1. Locations of all samples across western Canada from which specimens in the present study were recovered, color-coded by their terrane affinity. Select localities containing particularly productive sections are labeled by name. The western margin of Laurentia is in blue, including the Williston Lake sections. The Stikine Terrane is in green, including the Mount Sinwa and Hill 4308 sections. The Wrangell Terrane is in purple, including the Kyuquot Sound and Kennecott Point sections. The displayed extent of each terrane is from Colpron and Nelson (2011).
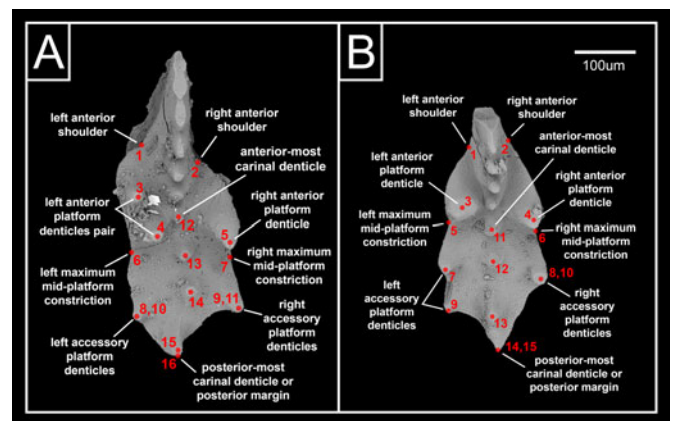

Figure 2. Geometric landmark models for (A) *Mockina* ex gr. *carinata* and (B) *Mockina* ex gr. *englandi* displayed on example specimens.

primarily differentiated from *M. carinata* by possessing only a single pair of large anterior platform denticles (one on each side of the element), typically resulting in a comparatively more bilaterally symmetric platform outline (Fig. 2B). Although *M. englandi* was originally defined by specimens displaying an ovoid platform, an abundance of specimens have since been recovered across western Canada that exhibit the strong anterior platform denticle pair, but with a wide variety of platform shapes. These varieties that deviate from the original diagnosis have been referred to as *M.* cf. *englandi* (Lei et al. 2022). Initially, *M. englandi* was proposed to have developed from *M. carinata* in the late Norian via the loss of one anterior platform denticle (Orchard 1991b), but significant numbers of *M.* cf. *englandi* have subsequently been recovered from middle Norian strata. The present study does not differentiate *M.* cf. *englandi* from *M. englandi* for the purposes of analysis, resulting in *M.* ex gr. *englandi* being present in the middle Norian, late Norian, and Rhaetian. Similarly, the present study considers all specimens with the anterior platform denticle arrangement consistent with *M. carinata* as *M.* ex gr. *carinata*.

Morphometric techniques have been widely utilized in both biology and paleontology to investigate the geometric form of specimens (e.g., Bookstein 1991). The platform landmark analysis methodology employed by the present study follows that utilized by prior morphometric analyses of Late Pennsylvanian conodont pectiniform elements (Hogancamp et al. 2016; Hogancamp and Barrick 2018; Hogancamp 2020). This landmarking methodology emphasizes the positions of distinct anatomical features, in contrast to morphometric studies of conodont pectiniform elements that focus more on the traced outline of elements (Klapper and Foster 1986, 1993; Renaud and Girard 1999; Girard et al. 2007; Zimmerman et al. 2018; Guenser et al. 2019). The outline-focused methodology has the advantage of not requiring identification of many common point features, resulting in specimen pools for analysis that accommodate a greater degree of morphological variability, potentially even including multiple genera. This methodology also produces a more precise representation of an element's outline shape, but can overlook crucial variation that does not affect the outline, which the feature-focused method would better capture. Both methods have been shown to be equally effective in detecting the pectiniform morphological variation that distinguishes species of the Late Devonian *Palmatolepis winchelli* group when employed on the same specimen pool (Hogancamp and Manship 2016). Given the universally prominent denticulation observed in both *M.* ex gr. *carinata* and *M.* ex gr. *englandi*, the feature-focused methodology is more appropriate for the present study.

Two similar geometric landmark models are utilized for the two species in the present study, composed predominantly of Type 1 landmarks, as defined by Bookstein (1991). Type 1 landmarks are points readily identifiable as homologous between specimens by being defined by a discrete junction of anatomical features; Type 2 landmarks are points of reliable maxima/minima along a boundary, typically with biomechanical implications (Bookstein 1991). For *M.* ex gr. *carinata* (Fig. 2A), these landmarks are the anterior shoulders where the platform meets the blade (1, 2, Type 1), the positions of the large anterior platform denticles (3–5, Type 1), the points of maximum mid-platform constriction between the main and accessory platform denticles (6, 7, Type 2), smaller accessory platform denticles posterior of the main set (8–11, Type 1), the positions of the carina denticles (12–15, Type 1), and the posterior margin of the carina (16, Type 1). For *M.* ex gr. *englandi* (Fig. 2B), these landmarks are the

anterior shoulders where the platform meets the blade (1, 2, Type 1), the positions of the large anterior platform denticles (3, 4, Type 1), the points of maximum mid-platform constriction between the main and accessory platform denticles (5, 6, Type 2), smaller accessory platform denticles posterior of the main set (7–10, Type 1), the positions of the carina denticles (11–14, Type 1), and the posterior margin of the carina (15, Type 1).

For the landmark models to accommodate an adequately large specimen pool despite the variability in the number of carina and accessory platform denticles in both species, it is necessary that any "leftover" platform denticle landmarks are overlapped on the posterior-most platform denticle of the same side, and any "leftover" carina denticles are overlapped on the posterior margin of the carina (Fig. 2A,B). Any loss in the quantity of carina and accessory platform denticles would therefore be expressed in analytical results by the convergence and overlapping of those landmarks in question, and vice versa for any gain in denticle quantity. This overlapping and de-overlapping of landmark positions would not be easily confused with results reflecting other aspects of morphological variance. Specimens of *M.* ex gr. *carinata* where the large anterior platform denticle set is mirrored from the landmark model displayed in Figure 2B were flipped horizontally for consistent chirality. All landmarks across both geometric models are based on the positions of various features within each conodont element as seen in upper view (lying on base and denticles pointing up toward the camera). Other potentially important morphological features that are only visible in other views, such as denticle height, keel shape, and basal pit location, are therefore not considered in the present study. More complicated geometric models incorporating additional landmarks from lateral and lower views would be impractical for the present study given the large specimen pool size, but could be the focus of more targeted future investigations.

With the geometric landmark models as defined, the number of suitable specimens utilized in the present study totals 154 for *M.* ex gr. *carinata* and 339 for *M.* ex gr. *englandi* across all localities (Table 1, Supplementary Appendix). The primary criteria for including specimens in the present study was applicability of the respective geometric landmark models as defined above, as opposed to coherence with any species diagnoses. For example, specimens of both species required at least a single accessory platform denticle on each side to be included in the analyses, but all manner of platform shapes were included regardless of whether such forms are typical for *M. carinata*, *M. englandi*, or even other similar species within *Mockina*. The requirement for prominent accessory platform denticulation screens out juvenile *Mockina* specimens, as these features generally only develop in adulthood (e.g., Orchard 1983; Rigo et al. 2018). The juvenile forms of many *Mockina* species can be indistinguishable from one another (e.g., Orchard 1983; Rigo et al. 2018), so the inclusion of juveniles would have introduced unnecessary taxonomic confusion in the specimen-selection process. A more detailed exploration of *Mockina* taxa and phylogeny can be found in a number of past studies (Orchard 1983, 1991a,b, 1994, 2018; Orchard et al. 2007; Mazza et al. 2012; Rigo et al. 2018). Digital photographs were taken of each specimen using a Nikon SMZ1270 microscope with integrally connected Canon Vixia HF G20 camcorder. All photography was conducted at 120× magnification, and specimens were positioned at a consistent orientation. The JPEG files were converted to TPS files using the software TpsUtil (Rohlf 2010a), and then the positions of all landmarks were identified per specimen in the software TpsDig (Rohlf 2010b). Morphometric analyses

were conducted using the software MorphoJ (Klingenberg 2011). First, a generalized Procrustes analysis was conducted on each species dataset, which minimizes all variation in specimen position, size, and rotation, in order to conserve only variation in specimen shape. Then, a wireframe model was created for each species, where landmark points are linked in a consistent manner to better facilitate visualization of form changes.

Finally, eigenanalyses were conducted. Canonical variate analysis (CVA) is a specific discriminatory eigenanalysis that produces eigenvectors (canonical variates) that represent axes that maximize separation of sets in multivariate space, with the sets externally predefined by classifiers. CVA was utilized in the present study, with the age of each specimen binned into middle Norian, late Norian, or Rhaetian as the predefined classifier. Therefore, the canonical variates (CV 1, CV 2) represent the factors of morphological variance that most significantly differentiate these age bins, each responsible for a certain proportion of total variance and summing to 100%. Each individual specimen has an eigenscore for each eigenvector, reflecting its morphology relative to the rest of the specimen pool for the given morphological factor. The changes in form along the scaling of these canonical variates are displayed using the wireframe models across the ranges of eigenscores exhibited by the specimens, connecting each eigenvector to tangible qualities in morphology.

Results

CVA of Mockina ex gr. carinata with Age as the Group Classifier

Conducting a CVA on the *Mockina* ex gr. *carinata* specimen pool with age as the group classifier (middle Norian, late Norian, Rhaetian) results in CV 1 explaining 69% of variance maximizing separation between the three age bins, whereas CV 2 explains 31%. More positive eigenscores along the CV 1 axis correspond to forms with a broader platform width, additional accessory platform denticles, and a slightly shortened carina (Fig. 3). More positive eigenscores along the CV 2 axis correspond to forms with an elongated carina, additional carina denticles, a constricted midplatform between the anterior and accessory platform denticles, and posteriorly shifted accessory platform denticles (Fig. 3). A continuous range of specimens are observed across both CV axes, but generally the most positive CV 1 scores are from middle Norian specimens (Fig. 3). CV 1 scores are more negative in late Norian specimens, and most negative in Rhaetian specimens (Fig. 3). Specimens from the middle Norian have a mean CV 1 score of 1.69, with values more positive than that almost exclusively associated with middle Norian specimens (Fig. 3). Specimens from the late Norian have a mean CV 1 score of −0.09 (Fig. 3). Specimens from the Rhaetian have a mean CV 1 score of −1.52, with values more negative than that almost exclusively associated with Rhaetian specimens (Fig. 3). There is overlap among the three age bins along the CV 2 axis, and no considerable separation between middle Norian and Rhaetian ranges, but CV 2 scores more negative than −1.12 are exclusively associated with late Norian specimens (Fig. 3).

CVA of Mockina ex gr. englandi with Age as the Group Classifier

Conducting a CVA on the *Mockina* ex gr. *englandi* specimen pool with age as the group classifier (middle Norian, late Norian, Rhaetian) results in CV 1 explaining 73% of variance maximizing
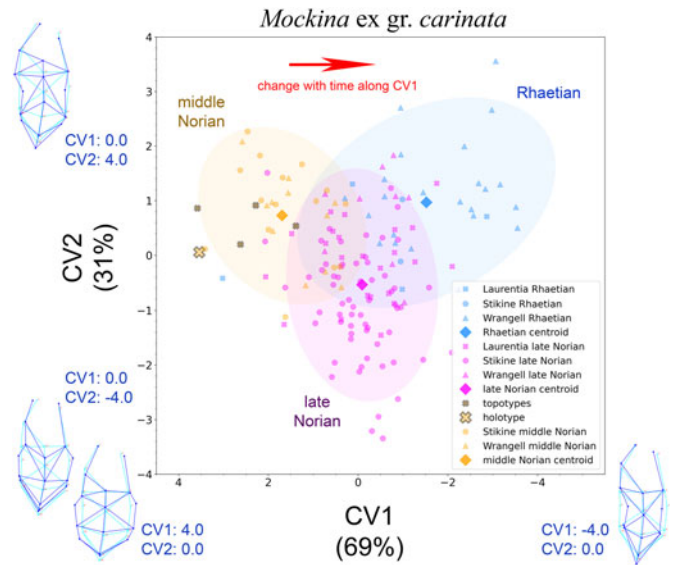

Figure 3. Canonical variate analysis (CVA) biplots for *Mockina* ex gr. *carinata* with age as the group classifier. The percentages along each axis label refers to the proportion of variance explained by each eigenvector. Also plotted for each age bin is a centroid representing the mean values of each age bin along both axes, and ellipses representing 2σ from each centroid. Dark blue wireframe models illustrate the extremes of each CV eigenscore still exhibited by natural specimens, overlaid on light blue wireframe models where all CV eigenscores are zero.

separation between the three age bins, whereas CV 2 explains 27%. More positive eigenscores along the CV 1 axis correspond to forms with a narrower platform width, an elongated carina, and additional carina denticles (Fig. 4). More positive eigenscores along the CV 2 axis correspond to forms with a shortened carina, a posterior carina curvature, and posteriorly shifted accessory platform denticles on the concave side of said curvature
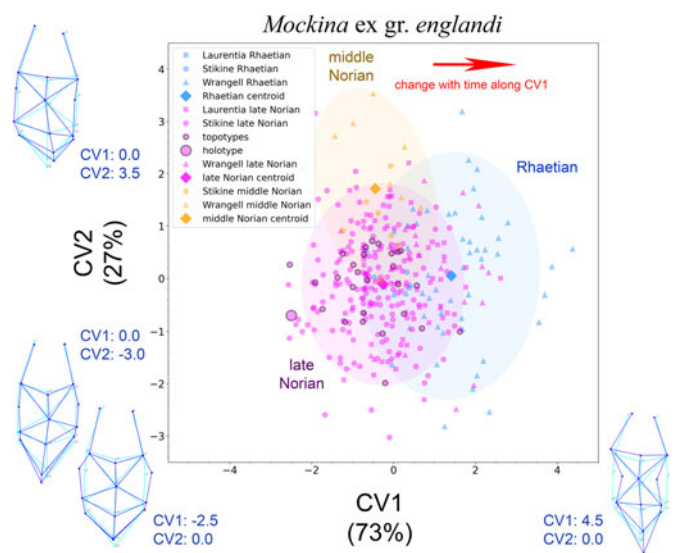

Figure 4. Canonical variate analysis (CVA) biplots for *Mockina* ex gr. *englandi* with age as the group classifier. The percentages along each axis label refers to the proportion of variance explained by each eigenvector. Also plotted for each age bin is a centroid representing the mean values of each age bin along both axes, and ellipses representing 2σ from each centroid. Dark blue wireframe models illustrate the extremes of each CV eigenscore still exhibited by natural specimens, overlaid on light blue wireframe models where all CV eigenscores are zero.

(Fig. 4). A continuous range of specimens are observed across both CV axes, but generally the most positive CV 1 scores are from Rhaetian specimens, whereas middle Norian and late Norian specimens tend to have more negative scores (Fig. 4). Specimens from the middle Norian have a mean CV 1 score of −0.45, whereas specimens from the late Norian have a mean CV 1 score of −0.26, with considerable overlap between the ranges of these two groups (Fig. 4). Specimens from the Rhaetian have a mean CV 1 score of 1.41, with values more positive than that almost exclusively associated with Rhaetian specimens (Fig. 4). There is overlap among the three age bins along the CV 2 axis, and no considerable separation between late Norian and Rhaetian ranges, but middle Norian specimens tend toward more positive values (Fig. 4). It is notable that overall separation of age bins for *M.* ex gr. *englandi* morphologies is less than that observed for *M.* ex gr. *carinata* (Figs. 3, 4).

Discussion

Evidence for Morphotype Origination or Subspeciation

It is notable that for both *Mockina* ex gr. *carinata* and *Mockina* ex gr. *englandi*, the holotype of each species has extreme CV 1 eigenscores far from the mean, with both late Norian and Rhaetian forms of *M.* ex gr. *carinata* progressing to more negative values than that of the middle Norian holotype, and Rhaetian forms of *M.* ex gr. *englandi* progressing to more positive values than that of the late Norian holotype (Figs. 3, 4). Although the holotype of *M. englandi* is generally assumed to be late Norian, the lack of independent age constraints for the specimen means it could potentially be Rhaetian instead (Orchard 1991b). Based on the present study, the broader platform of the *M. englandi* holotype indicates that it resembles late Norian forms much more than Rhaetian forms (Fig. 4). The topotypes of *M.* ex gr. *carinata* are largely restricted to more positive CV 1 values indicative of the middle Norian forms of that species (Fig. 3), whereas the topotypes of *M.* ex gr. *englandi* span a large portion of the CV 1 axis variability but largely do not encroach into the more positive CV 1 values indicative of the Rhaetian forms of that species (Fig. 4). There are multiple potential explanations for the outlier morphologies of both holotypes. It is possible that the holotypes were selected precisely due to their aberrant forms, being distinct within the species. Alternatively, they may have been selected due to their particularly broad platforms, as reflected in their CV 1 eigenscores. The arrangement and height of platform denticles are key to the diagnoses of both species, such that a specimen with a broader platform would likely display these features more clearly. Nevertheless, both species are now defined by holotypes that are not representative of the species as a whole in terms of platform width, with CV 1 distribution as evidence for morphotype origination or subspeciation away from the holotypes toward reduced platform morphologies across the NRB.

From the CVA results, thresholds of platform width can be determined for both *M.* ex gr. *carinata* and *M.* ex gr. *englandi*, past which specimens can be reliably identified as Rhaetian in age. For *M.* ex gr. *carinata*, the most negative CV 1 score for a late Norian specimen is −2.10, with all values more negative than that associated with Rhaetian specimens (Figs. 3, 5A). This CV 1 score threshold represents a mid-platform length to breadth ratio of 2.9:1. For *M.* ex gr. *englandi*, the most positive CV 1 score for a late Norian specimen is 2.61, with all values more positive than that associated with Rhaetian specimens (Figs. 4, 5B). This
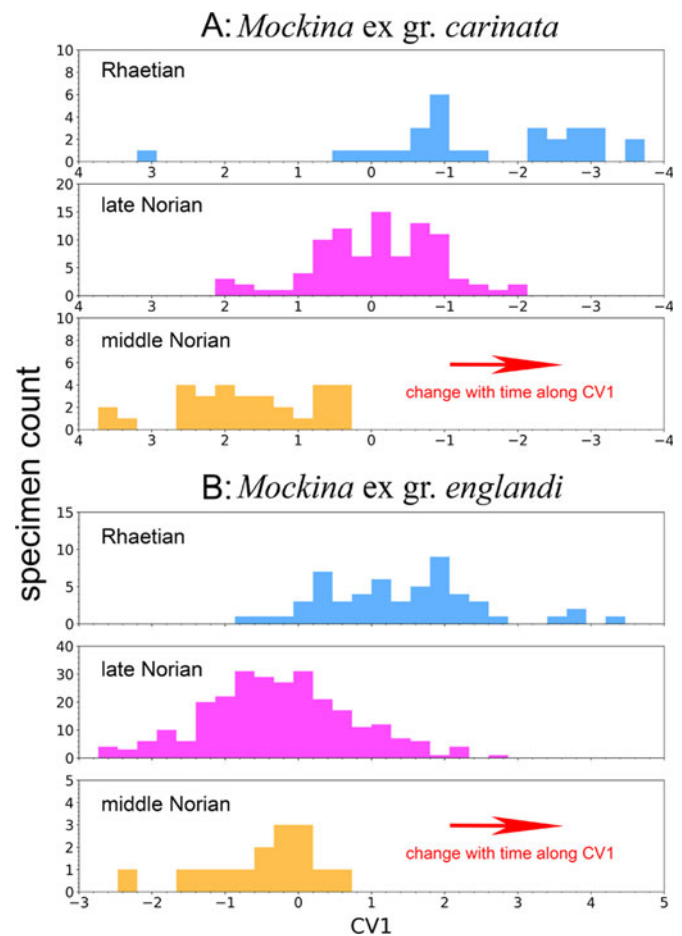

Figure 5. CV 1 eigenscore distribution from canonical variate analysis (CVA) with age as the group classifier of (A) *Mockina* ex gr. *carinata* and (B) *Mockina* ex gr. *englandi* for specimens of each age bin.

CV 1 score threshold represents a mid-platform length to breadth ratio of 3.1:1. Therefore, specimens of these two species with ratios greater than this threshold ratio of ∼3:1 can be reliably identified as Rhaetian in age; however, given the overlap between the Norian and Rhaetian CV 1 score ranges of both species, specimens displaying ratios lower than ∼3:1 are not exclusively Norian (Figs. 3–5). These determinations will have biostratigraphic utility for future studies involving Norian and Rhaetian conodonts from the Canadian Cordillera, and with wider testing may even prove to have global utility.

Correlation to the NRB at Kennecott Point

The exact position of the NRB remains uncertain and contentious, with a number of different biostratigraphic proxies having been proposed and utilized, despite the asynchroneity between some if not all of these proxies (e.g., Carter and Orchard 2007; Orchard et al. 2007; Krystyn 2010; Rigo et al. 2016, 2020; Taylor et al., 2021; Lei et al. 2022; Rigo and Campbell 2022). As such, understanding the timing of pectiniform platform reduction in *M.* ex gr. *carinata* and *M.* ex gr. *englandi* requires precise correlation of conodont morphology shifts to these various NRB proxies. Many of the specimens utilized in the present study do not have age constraints more precise than their age bins (middle Norian, late Norian, Rhaetian), but the composite Kennecott

Point section on Haida Gwaii compiled by Carter and Orchard (2007) represents an opportunity to extract a subset of the specimen pool and observe how the forms of both these species change within a continuous stratigraphic section. These specimens can be situated precisely within the Kennecott Point section, spanning a large variety of stratigraphic positions relative to a well-constrained NRB primarily defined by the first occurrence of the Rhaetian radiolarian *Proparvicingula moniliformis* at 10.7 m, supported by the slightly higher first occurrence of the Rhaetian conodont *Mockina mosheri* morphotype A at 13.0 m (Carter and Orchard 2007; Fig. 6).

Lower in the Kennecott Point section (0.9 m in Fig. 6), Ward et al. (2001, 2004) previously identified the NRB as defined by the conspicuous disappearance of the bivalve genus *Monotis*, coinciding with a positive excursion in $\delta^{13}C$ values of organic carbon, interpreted together to indicate environmental stress via deoxygenation. The positive excursion of ~1.5‰ is arguably dubious, because it is largely defined by a single data point. However, the disappearance of *Monotis*, which often dominates among Norian fauna, is unambiguous (e.g., Ward et al. 2001, 2004; Wignall et al. 2007; Rigo et al. 2016, 2020). The last occurrence of *Monotis* has been used as a proxy approximating the NRB in many sections globally, despite being understood to be somewhat

Figure 6. CV 1 eigenscores from canonical variate analysis (CVA) with age as the group classifier of *Mockina* ex gr. *carinata* and *Mockina* ex gr. *englandi* across the Kennecott Point section from Carter and Orchard (2007). The Norian/Rhaetian boundary (NRB) is drawn at the base of the *Proparvicingula moniliformis* Zone. The range of CV 1 eigenscores exclusively exhibited by Rhaetian specimens are highlighted in red for each species. A linear line of best fit is displayed in purple for *M.* ex gr. *carinata*, and in green for *M.* ex gr. *englandi*, with each regression surrounded by its respective 98% confidence interval.

older than many other proxies (e.g., Ward et al. 2001, 2004; Wignall et al. 2007; Rigo et al. 2016, 2020; Lei et al. 2022). The Kennecott Point section also hosts a rare occurrence of *Misikella posthernsteini* in Panthalassa, at ~77 m extrapolating from Figure 6 (Orchard 1991a; Carter and Orchard 2007; Orchard et al. 2007). The first occurrence of this conodont species is widely used to mark the NRB in Tethys (e.g., Krystyn 2010; Rigo et al. 2016, 2018; Karádi et al. 2020), but co-occurrence with the ammonoid *Chorisoceras nobile* at Kennecott Point suggests this occurrence of *M. posthernsteini* is well into the Rhaetian Stage (Orchard 1991a; Tipper et al. 1994; Carter and Orchard 2007; Orchard et al. 2007).

Deposition at the Kennecott Point section has been interpreted as having occurred in an open ocean slope setting (e.g., Desrochers and Orchard 1991; Kasprak et al. 2015; Schoepfer et al. 2016). A number of past studies have utilized a wide variety geochemical proxies to investigate the paleoenvironmental conditions spanning the Norian–Hettangian interval of Kennecott Point and generally proposed expanding anoxic conditions and biotic distress at the Triassic/Jurassic boundary, as well as for variable portions of the late Rhaetian, but did not suggest that these disturbances extend back to the NRB (e.g., Ward et al. 2001, 2004; Williford et al. 2007, 2009; Kasprak et al. 2015; Schoepfer et al. 2016).

The occurrence of reduced platform morphologies in *M.* ex gr. *carinata* begins at 16.8 m within the Kennecott Point section, and in *M.* ex gr. *englandi* at 18.0 m, both situated higher than the radiolarian-defined NRB at 10.7 m (Fig. 6). Although these reduced platform morphologies emerge in the Rhaetian, it is notable that the late Norian forms still occur in the highest conodont sample recovered from the section (Fig. 6). Although limited by the absence of middle Norian specimens at Kennecott Point, the lack of a clear gradual trend toward more negative CV 1 values for *M.* ex gr. *carinata* may suggest pectiniform platform reduction did not occur continuously from the middle Norian through to the Rhaetian as could be interpreted from the CVA results, but perhaps stepwise instead. Although the emergence of reduced platform morphologies in both conodont species occur somewhat later than other NRB proxies, this shift is likely still associated with the NRB, as all these biotic changes are clustered much closer to each other stratigraphically than to the Triassic/Jurassic boundary located significantly higher in the Kennecott Point section (99.9 m, extrapolating from Fig. 6) (Ward et al. 2001, 2004; Carter and Orchard 2007; Williford et al. 2007, 2009; Kasprak et al. 2015; Schoepfer et al. 2016). The apparent asynchroneity of response to the disturbance around the NRB could be interpreted as evidence for different biotic groups having differing degrees of susceptibility to the environmental changes associated with the boundary, as motile organisms such as conodonts (e.g., Briggs et al. 1983; Purnell 1995) were perhaps able to endure the abiotic stress better than benthic, sessile communities.
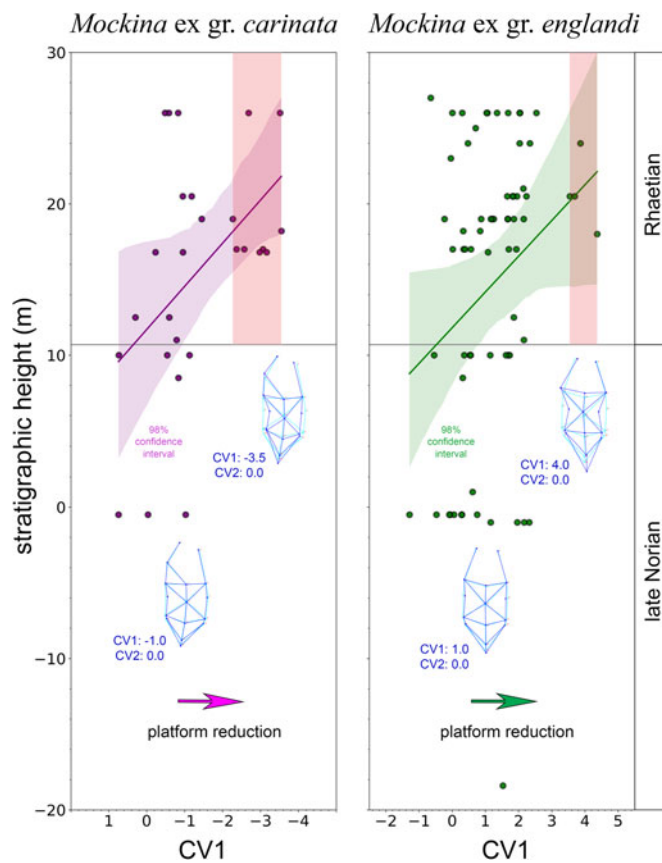
Paleoenvironmental Implications

Shifts in conodont element morphology may reflect the changing needs of food resource acquisition, as it has been widely suggested that conodont elements comprised a feeding apparatus that functioned by grasping and masticating food material (e.g., Briggs et al. 1983; Purnell and von Bitter 1992; Purnell 1993, 1995; Donoghue and Purnell 1999; Purnell and Jones 2012; Martínez-Pérez et al. 2014b, 2016; Kelz et al. 2023). Conodont survivorship across the Permian/Triassic mass extinction was remarkably high, and this may have been due in some degree

to adaptations made in response to the extreme environmental pressures of this time interval, such as decreasing pectiniform element size in response to previous food sources becoming compromised (e.g., Clark et al. 1986; Luo et al. 2006; Schaal et al. 2016; Zhang et al. 2017; Lai et al. 2018). The platform reduction observed across the NRB in both *M.* ex gr. *carinata* and *M.* ex gr. *englandi*, even when controlling for specimen size, may similarly reflect a response to environmental disturbance impacting food availability.

While changes in the overall size or complexity of conodont elements can indicate some manner of disruption to feeding habits, the presence/absence of platforms on pectiniform elements is not wholly dependent on element size, but instead likely reflects diversity in ecological niche (e.g., Ginot and Goudemand 2019). Therefore, the platform width reduction observed across the NRB may allow for more specific inferences regarding mode of life shifts, due to the greater linkage between morphology and function, than consideration of element size alone. It has long been proposed that pectiniform conodont elements were somewhat analogous in function to mammalian molars, in the sense of being specialized for grinding motions as opposed to grasping or shearing motions, based on multiple lines of evidence, including growth allometry, patterns of microwear, and occlusion modeling (e.g., Purnell 1993, 1995; Donoghue and Purnell 1999; Purnell and Jones 2012; Martínez-Pérez et al. 2014b; Kelz et al. 2023). Although food sources for conodonts remain largely speculative, Martínez-Pérez et al. (2016) demonstrate how the gradual evolutionary expansion of a wider platform in the conodont genus *Polygnathus* would work to distribute stress such that greater forces can be endured during element function, opening up the viability of processing harder materials. The platform reduction in pectiniform elements across the NRB, both intraspecifically in Panthalassa and intergenerically in Tethys, may therefore indicate a trend in which some conodonts shifted away from mineralized food sources in the Rhaetian. This response may have been due to a change in availability of different food sources as compared with the Norian.

An alternative driver for the pectiniform platform reduction across the NRB would be elevated bioapatite mineralization pressure, directly inhibiting the growth of robust conodont elements. However, there is no evidence of phosphatic mineralization suppression around the Norian–Rhaetian interval. For example, at Williston Lake in British Columbia, the presence of abiotically precipitated phosphatic pebble conglomerate beds commonly mark the Rhaetian and are interpreted to indicate spreading anoxic conditions off the western margin of Laurentia in the leadup to the ETME (Larina et al. 2019).

Global carbonate mineralization suppression has long been associated with the ETME, caused by ocean acidification linked to the enhanced volcanic outgassing of CAMP emplacement (e.g., Stanley 1988; Hautmann 2004). The decline of faunal groups such as bivalves and corals at the NRB may suggest that this carbonate suppression began to occur much earlier, albeit to a lesser degree (Ward et al. 2001, 2004; Flügel and Kiessling 2002; Stanley 2003; Wignall et al. 2007; Rigo et al. 2016, 2020; Lei et al. 2022). If carbonate biomineralization was suppressed in these groups, it is possible that the same pressures were being exerted on potential conodont food sources at the NRB. A decrease in the prevalence of mineralized food sources would render robust pectiniform elements unnecessary. This interpretation involving carbonate suppression would support the hypothesis of large-scale CO_2 emission being the causal mechanism of the environmental disturbance at the NRB, as has been previously proposed by a number of studies (e.g., Korte et al. 2003; Callegaro et al. 2012; Tackett et al. 2014; Zaffani et al. 2017; Rigo et al. 2020). However, with the absence of any large igneous province convincingly associated with the NRB, the source of this hypothetical episode of enhanced greenhouse gas emission remains speculative.

Conclusions

Morphometric analyses conducted on the pectiniform elements of the conodont species *Mockina* ex gr. *carinata* and *Mockina* ex gr. *englandi* spanning the middle Norian through Rhaetian of many localities in western Canada demonstrate that both species exhibit platform width reduction across the NRB. In regard to *M.* ex gr. *carinata*, this platform reduction occurs sequentially from middle Norian to late Norian to Rhaetian, whereas in *M.* ex gr. *englandi*, the shift only occurs across the NRB. Overall, *M.* ex gr. *englandi* seems to be more conservative in terms of morphological change than *M.* ex gr. *carinata*, as the former's morphologies do not separate the age bin clusters as prominently as the latter's along CV axes. With the reduced platform morphologies of both species arising in the Rhaetian, specimens of *M.* ex gr. *carinata* and *M.* ex gr. *englandi* from the Canadian Cordillera that have a mid-platform length to breadth ratio greater than 3:1 can be reliably identified as Rhaetian in age. It is notable that many of the Norian forms are still conserved across the NRB, so specimens with a lower ratio can still potentially be Rhaetian. At Kennecott Point specifically, the emergence of the reduced platform morphologies does not occur until somewhat after many other disturbances and biostratigraphic proxies associated with the NRB, such as the disappearance of the bivalve genus *Monotis* (Ward et al. 2001, 2004). This new intraspecific platform reduction observed in Panthalassa is consistent with intergeneric trends largely observed in many conodonts from the Tethys (e.g., Orchard et al. 2007; Giordano et al. 2010; Mazza et al. 2012; Rigo et al. 2018; Karádi et al. 2020; Du et al. 2021, 2023), suggesting that these morphological trends (as well as their driving mechanisms) are global in extent. A potential explanation for the pectiniform platform reduction is a shift in primary diet away from hard materials, perhaps reflecting elevated carbonate mineralization pressure beginning around the NRB. Biomineralization suppression is typically associated with the ETME (e.g., Stanley 1988; Hautmann 2004), but if this pressure began at a lesser severity as far back as the NRB, this would support the concept of a drawn-out multiphase mass extinction leading into the end-Triassic.

Literature Cited

Belasky, P., C. H. Stevens, and R. A. Hanger. 2002. Early Permian location of western North American terranes based on brachiopod, fusulinid, and coral biogeography. *Palaeogeography, Palaeoclimatology, Palaeoecology* 179:245–266.

Beranek, L. P., and J. K. Mortensen. 2011. The timing and provenance record of the Late Permian Klondike orogeny in northwestern Canada and arc-continent collision along western North America. *Tectonics* 30:1–23.

Blackburn, T. J., P. E. Olsen, S. A. Bowring, N. M. McLean, D. V. Kent, J. Puffer, G. McHone, E. T. Rasbury, and M. Et-Touhami. 2013. Zircon U-Pb geochronology links the end-Triassic extinction with the Central Atlantic Magmatic Province. *Science* 340:941–945.

Bookstein, F. P. 1991. *Morphometric tools for landmark data: geometry and biology.* Cambridge University Press, Cambridge.

Briggs, D. E. G., E. N. K. Clarkson, and R. J. Aldridge. 1983. The conodont animal. *Lethaia* 16:1–14.

Callegaro, S., M. Rigo, M. Chiaradia, and A. Marzoli. 2012. Latest Triassic marine Sr isotopic variations, possible causes and implications. *Terra Nova* 24:130–135.

Carter, E. S., and M. J. Orchard. 2007. Radiolarian–conodont–ammonoid intercalibration around the Norian–Rhaetian boundary and implications for trans-Panthalassan correlation. *Albertiana* 36:149–163.

Caruthers, A. H., S. M. Marroquín, D. R. Gröcke, M. L. Golding, M. Aberhan, T. R. Them, Y. P. Veenma, et al. 2022. New evidence for a long Rhaetian from a Panthalassan succession (Wrangell Mountains, Alaska) and regional differences in carbon cycle perturbations at the Triassic–Jurassic transition. *Earth and Planetary Science Letters* 577:117262.

Clark, D. L. 1983. Extinction of conodonts. *Journal of Paleontology* 57:652–661.

Clark, D. L., C. Y. Wang, C. J. Orth, and J. S. Gilmore. 1986. Conodont survival and low iridium abundances across the Permian–Triassic boundary in south China. *Science* 233:984–986.

Colpron, M., and J. Nelson. 2011. *A Digital Atlas of Terranes for the Northern Cordillera.* BCGS Geofile 11. British Columbia Ministry of Energy and Mines.

Colpron, M., and J. L. Nelson. 2009. A Palaeozoic Northwest Passage: incursion of Caledonian, Baltican and Siberan terranes into eastern Panthalassa, and the early evolution of the North American Cordillera. *Geological Society Special Publication* 318:273–307.

Davies, J. H. F. L., A. Marzoli, H. Bertrand, N. Youbi, M. Ernesto, and U. Schaltegger. 2017. End-Triassic mass extinction started by intrusive CAMP activity. *Nature Communications* 8:15596.

Desrochers, A., and M. J. Orchard. 1991. Stratigraphic revisions and carbonate sedimentology of the Kunga Group (Upper Triassic–Lower Jurassic), Queen Charlotte Islands, British Columbia. *In* G. J. Woodsworth, ed. *Evolution and hydrocarbon potential of the Queen Charlotte Basin, British Columbia.* Geological Survey of Canada Paper 90-10:163–172.

Donoghue, P. C. J., and M. A. Purnell. 1999. Mammal-like occlusion in conodonts. *Paleobiology* 25:58–74.

Du, Y., A. Bertinelli, X. Jin, Z. Shi, V. Karádi, H. Yin, L. Han, Q. Wu, and M. Rigo. 2020a. Integrated conodont and radiolarian biostratigraphy of the upper Norian in Baoshan Block, Southwestern China. *Lethaia* 53:533–545.

Du, Y., M. Chiari, V. Karádi, A. Nicora, T. Onoue, J. Pálfy, G. Roghi, Y. Tomimatsu, and M. Rigo. 2020b. The asynchronous disappearance of conodonts: new constraints from Triassic–Jurassic boundary sections in the Tethys and Panthalassa. *Earth-Science Reviews* 203:103176.

Du, Y., T. Onoue, V. Karádi, I. S. Williams, and M. Rigo. 2021. Evolutionary process from *Mockina bidentata* to *Parvigondolella andrusovi*: evidence from the Pizzo Mondello section, Sicily, Italy. *Journal of Earth Science* 32:667–676.

Du, Y., T. Onoue, Y. Tomimatsu, Q. Wu, and M. Rigo. 2023. Lower Jurassic conodonts from the Inuyama area of Japan: implications for conodont extinction. *Frontiers in Ecology and Evolution* 11:113578.

Ernst, R. E., and K. L. Buchan, eds. 2001. Mantle plumes: their identification through time. *Geological Society of America Special Paper* 352:1–593.

Flügel, E., and W. Kiessling. 2002. Patterns of Phanerozoic reef crises. *SEPM Special Publication* 72:691–733.

Ginot, S., and N. Goudemand. 2019. Conodont size, trophic level, and the evolution of platform elements. *Paleobiology* 45:458–468.

Giordano, N., M. Rigo, G. Ciarapica, and A. Bertinelli. 2010. New biostratigraphical constraints for the Norian/Rhaetian boundary: data from Lagonegro Basin, Southern Apennines, Italy. *Lethaia* 43:573–586.

Girard, C., S. Renaud, and R. Feist. 2007. Morphometrics of the Late Devonian conodont genus *Palmatolepis*: phylogenetic, geographical and ecological contributions of a generic approach. *Journal of Micropalaeontology* 26:61–72.

Guenser, P., L. Souquet, S. Dolédec, M. Mazza, M. Rigo, and N. Goudemand. 2019. Deciphering the roles of environment and development in the evolution of a Late Triassic assemblage of conodont elements. *Paleobiology* 45:440–457.

Hallam, A. 2002. How catastrophic was the end-Triassic mass extinction? *Lethaia* 35:147–157.

Hautmann, M. 2004. Effect of end-Triassic CO_2 maximum on carbonate sedimentation and marine mass extinction. *Facies* 50:257–261.

Hesselbo, S. P., S. A. Robinson, F. Surlyk, and S. Piasecki. 2002. Terrestrial and marine extinction at the Triassic–Jurassic boundary synchronized with major carbon-cycle perturbation: a link to initiation of massive volcanism? *Geology* 30:251–254.

Hogancamp, N., and J. Barrick. 2018. Morphometric analysis and taxonomic revision of North American species of the *Idiognathodus eudoraensis* Barrick, Heckel, and Boardman, 2008 group (Missourian, Upper Pennsylvanian Conodonts). *Bulletins of American Paleontology* 395–396:35–69.

Hogancamp, N. J. 2020. P1 element morphological variability within the Late Pennsylvanian asymmetrical *Idiognathodus* clade from the midcontinent, U.S.A. and implications for ontogeny, taxonomy, phylogeny, and function. *Palaeogeography, Palaeoclimatology, Palaeoecology* 549:109090.

Hogancamp, N. J., and L. L. Manship. 2016. Comparison of morphometric techniques and the ability to accurately reconstruct the form and distinguish between species of the *Palmatolepis winchelli* group—Conodonta, Upper Devonian. *Micropaleontology* 62:439–451.

Hogancamp, N. J., J. E. Barrick, and R. E. Strauss. 2016. Geometric morphometric analysis and taxonomic revision of the Gzhelian (Late Pennsylvanian) conodont *Idiognathodus* simulator from North America. *Acta Palaeontologica Polonica* 61:477–502.

Johnston, S. T. 2008. The cordilleran ribbon continent of North America. *Annual Review of Earth and Planetary Sciences* 36:495–530.

Johnston, S. T., and G. D. Borel. 2007. The odyssey of the Cache Creek terrane, Canadian Cordillera: implications for accretionary orogens, tectonic setting of Panthalassa, the Pacific superwell, and break-up of Pangea. *Earth and Planetary Science Letters* 253:415–428.

Jones, D. L., N. J. Silberling, and J. Hillhouse. 1977. Wrangellia—a displaced terrane in northwestern North America. *Canadian Journal of Earth Sciences* 14:2565–2577.

Karádi, V., A. Cau, M. Mazza, and M. Rigo. 2020. The last phase of conodont evolution during the Late Triassic: integrating biostratigraphic and phylogenetic approaches. *Palaeogeography, Palaeoclimatology, Palaeoecology* 549:109144.

Kasprak, A. H., J. Sepúlveda, R. Price-Waldman, K. H. Williford, S. D. Schoepfer, J. W. Haggart, P. D. Ward, R. E. Summons, and J. H. Whiteside. 2015. Episodic photic zone euxinia in the northeastern Panthalassic Ocean during the end-Triassic extinction. *Geology* 43:307–310.

Kelz, V., P. Guenser, M. Rigo, and E. Jarochowska. 2023. Growth allometry and dental topography in Upper Triassic conodonts support trophic differentiation and molar-like element function. *Paleobiology* 49:1–19.

Kent, D. V., and E. Irving. 2010. Influence of inclination error in sedimentary rocks on the Triassic and Jurassic apparent pole wander path for North America and implications for Cordilleran tectonics. *Journal of Geophysical Research: Solid Earth* 115(10):1–25.

Klapper, G., and C. T. Foster. 1986. Quantification of outlines in Frasnian (Upper Devonian) platform conodonts. *Canadian Journal of Earth Sciences* 23:1214–1222.

Klapper, G., and C. T. Foster. 1993. Shape analysis of Frasnian species of the Late Devonian conodont genus *Palmatolepis*. *Journal of Paleontology Memoir* 32:1–35.

Klingenberg, C. P. 2011. MorphoJ: an integrated software package for geometric morphometrics. *Molecular Ecology Resources* **11**:353–357.

Korte, C., H. W. Kozur, P. Bruckschen, and J. Veizer. 2003. Strontium isotope evolution of Late Permian and Triassic seawater. *Geochimica et Cosmochimica Acta* **67**:47–62.

Kozur, H. W. 1989a. Significance of events in conodont evolution for the Permian and Triassic stratigraphy. *Courier Forschungsinstitut Senckenberg* **117**:385–408.

Kozur, H. W. 1989b. The taxonomy of the Gondolellid conodonts in the Permian and Triassic. *Courier Forschungs-Institut Senckenberg* **117**:409–469.

Krystyn, L. 2010. Decision report on the defining event for the base of the Rhaetian Stage. *Albertiana* **38**:11–12.

Lai, X., H. Jiang, and P. B. Wignall. 2018. A review of the Late Permian–Early Triassic conodont record and its significance for the end-Permian mass extinction. *Revue de Micropaleontologie* **61**:155–164.

Larina, E., D. J. Bottjer, F. A. Corsetti, J. P. Zonneveld, A. J. Celestian, and J. V. Bailey. 2019. Uppermost Triassic phosphorites from Williston Lake, Canada: link to fluctuating euxinic-anoxic conditions in northeastern Panthalassa before the end-Triassic mass extinction. *Scientific Reports* **9**:18790.

Lei, J. Z. X., M. L. Golding, and J. M. Husson. 2022. Paleoenvironmental interpretation of the Late Triassic Norian–Rhaetian boundary interval in the Whitehorse Trough (Stikine Terrane, northern Canadian Cordillera). *Palaeogeography, Palaeoclimatology, Palaeoecology* **608**:111306.

Lucas, S. G. 2018. Late Triassic ammonoids: distribution, biostratigraphy and biotic events. Pp. 237–261 in L. H. Tanner, ed. *The Late Triassic world: Earth in a time of transition*. Topics in Geobiology 46. Springer, Cham, Switzerland.

Luo, G., X. Lai, H. Jiang, and K. Zhang. 2006. Size variation of the end Permian conodont *Neogondolella* at Meishan Section, Changxing, Zhejiang and its significance. *Science in China, Series D: Earth Sciences* **49**:337–347.

Martínez-Pérez, C., P. Plasencia, B. Cascales-Miñana, M. Mazza, and H. Botella. 2014a. New insights into the diversity dynamics of Triassic conodonts. *Historical Biology* **26**:591–602.

Martínez-Pérez, C., E. J. Rayfield, M. A. Purnell, and P. C. J. Donoghue. 2014b. Finite element, occlusal, microwear and microstructural analyses indicate that conodont microstructure is adapted to dental function. *Palaeontology* **57**:1059–1066.

Martínez-Pérez, C., E. J. Rayfield, H. Botella, and P. C. J. Donoghue. 2016. Translating taxonomy into the evolution of conodont feeding ecology. *Geology* **44**:247–250.

Marzoli, A., P. R. Renne, E. M. Piccirillo, M. Ernesto, G. Bellieni, and A. De Min. 1999. Extensive 200-million-year-old continental flood basalts of the Central Atlantic Magmatic Province. *Science* **284**:616–618.

Marzoli, A., H. Bertrand, K. B. Knight, S. Cirilli, N. Buratti, C. Vérati, S. Nomade, *et al.* 2004. Synchrony of the Central Atlantic Magmatic Province and the Triassic–Jurassic boundary climatic and biotic crisis. *Geology* **32**:973–976.

Mazza, M., M. Rigo, and M. Gullo. 2012. Taxonomy and biostratigraphic record of the Upper Triassic conodonts of the Pizzo Mondello section (western Sicily, Italy), GSSP candidate for the base of the Norian. *Rivista Italiana di Paleontologia e Stratigrafia* **118**:85–130.

Mihalynuk, M. G., J. A. Nelson, and L. J. Diakow. 1994. Cache Creek Terrane entrapment: oroclinal paradox within the Canadian Cordillera. *Tectonics* **13**:575–595.

Monger, J. W. H., and C. A. Ross. 1971. Distribution of Fusulinaceans in the Western Canadian Cordillera. *Canadian Journal of Earth Sciences* **8**:259–278.

Orchard, M. J. 1983. *Epigondolella* populations and their phylogeny and zonation in the Upper Triassic. *Fossils and Strata* **15**:177–192.

Orchard, M. J. 1991a. Late Triassic conodont biochronology and biostratigraphy of the Kunga Group, Queen Charlotte Islands, British Columbia. *In* G. J. Woodsworth, ed. *Evolution and hydrocarbon potential of the Queen Charlotte Basin, British Columbia*. Geological Survey of Canada Paper 90–10:173–193.

Orchard, M. J. 1991b. Upper Triassic conodont biochronology and new index species from the Canadian Cordillera. *Geological Survey of Canada Bulletin* **417**:299–335.

Orchard, M. J. 1994. Late Triassic (Norian) conodonts from Peru. Pp. 203–208 in G. D. Stanley Jr., ed. *Paleontology and stratigraphy of Triassic to Jurassic rocks of the Peruvian Andes*. Palaeontographica Abteilung A Band 233 Lieferung 1–6. Schweizerbart Science Publishers, Stuttgart.

Orchard, M. J. 2018. The lower–middle Norian (Upper Triassic) boundary: new conodont taxa and a refined biozonation. Pp. 165–193 in J. D. Over and C. H. Henderson, eds. *Conodont studies dedicated to the careers and contributions of Anita Harris, Glen Merrill, Carl Rexroad, Walter Sweet, and Bruce Wardlaw. Bulletins of American Paleontology* 395–396.

Orchard, M. J., E. S. Carter, S. G. Lucas, and D. G. Taylor. 2007. Rhaetian (Upper Triassic) conodonts and radiolarians from New York Canyon, Nevada, USA. *Albertiana* **35**:59–65.

Pálfy, J., A. Demény, J. Haas, E. S. Carter, Á. Görög, D. Halász, A. Oravecz-Scheffer, *et al.* 2007. Triassic–Jurassic boundary events inferred from integrated stratigraphy of the Csovár section, Hungary. *Palaeogeography, Palaeoclimatology, Palaeoecology* **244**(1–4):11–33.

Purnell, M. A. 1993. Feeding mechanisms in conodonts and the function of the earliest vertebrate hard tissues. *Geology* **21**:375–377.

Purnell, M. A. 1995. Microwear on conodont elements and macrophagy in the first vertebrates. *Nature* **374**:798–800.

Purnell, M. A., and D. Jones. 2012. Quantitative analysis of conodont tooth wear and damage as a test of ecological and functional hypotheses. *Paleobiology* **38**:605–626.

Purnell, M. A., and P. H. von Bitter. 1992. Blade-shaped conodont elements functioned as cutting teeth. *Nature* **359**:629–631.

Raup, D. M., and J. J. Sepkoski. 1982. Mass extinctions in the marine fossil record. *Science* **215**:1501–1503.

Renaud, S., and C. Girard. 1999. Strategies of survival during extreme environmental perturbations: evolution of conodonts in response to the Kellwasser crisis (Upper Devonian). *Palaeogeography, Palaeoclimatology, Palaeoecology* **146**(1–4):19–32.

Rigo, M., and H. Campbell. 2022. Correlation between the Warepan/Otapirian and the Norian/Rhaetian stage boundary: implications of a global negative $\delta^{13}C_{org}$ perturbation. *New Zealand Journal of Geology and Geophysics* **65**:397–406.

Rigo, M., A. Bertinelli, G. Concheri, G. Gattolin, L. Godfrey, M. E. Katz, M. Maron, *et al.* 2016. The Pignola-Abriola section (southern Apennines, Italy): a new GSSP candidate for the base of the Rhaetian Stage. *Lethaia* **49**:287–306.

Rigo, M., M. Mazza, V. Karádi, and A. Nicora. 2018. New Upper Triassic conodont biozonation of the Tethyan realm. Pp. 189–235 in L. H. Tanner, ed. *The Late Triassic world: Earth in a time of transition*. Topics in Geobiology 46. Springer, Cham, Switzerland.

Rigo, M., T. Onoue, L. Tanner, S. G. Lucas, L. Godfrey, M. E. Katz, M. Zaffani, *et al.* 2020. The Late Triassic extinction at the Norian/Rhaetian boundary: biotic evidence and geochemical analysis. *Earth-Science Reviews* **204**:103180.

Rohlf, F. J. 2010a. TpsDig, Version 2.16. Department of Ecology and Evolution, State University of New York, Stony Brook. https://www.sbmorphometrics.org.

Rohlf, F. J. 2010b. TpsUtil, Version 1.46. Department of Ecology and Evolution, State University of New York, Stony Brook. https://www.sbmorphometrics.org.

Ruhl, M., and W. M. Kürschner. 2011. Multiple phases of carbon cycle disturbance from large igneous province formation at the Triassic–Jurassic transition. *Geology* **39**:431–434.

Schaal, E. K., M. E. Clapham, B. L. Rego, S. C. Wang, and J. L. Payne. 2016. Comparative size evolution of marine clades from the Late Permian through Middle Triassic. *Paleobiology* **42**:127–142.

Schoepfer, S. D., T. J. Algeo, P. D. Ward, K. H. Williford, and J. W. Haggart. 2016. Testing the limits in a greenhouse ocean: did low nitrogen availability limit marine productivity during the end-Triassic mass extinction? *Earth and Planetary Science Letters* **451**:138–148.

Sepkoski, J. J. 1981. A factor analytic description of the Phanerozoic marine fossil record. *Paleobiology* **7**:36–53.

Stanley, G. D. 1988. The history of early Mesozoic reef communities: a three-step process. *Palaios* **3**:170–183.

Stanley, G. D. 2003. The evolution of modern corals and their early history. *Earth-Science Reviews* **60**:195–225.

Stone, J. 1987. Review of investigative techniques used in the study of conodonts. Pp. 17–34 *in* R. L. Austin, ed. *Conodonts: investigative techniques and applications*. British Micropalaeontological Society Series. Ellis Horwood, Chichester, U.K.

Tackett, L. S., A. J. Kaufman, F. A. Corsetti, and D. J. Bottjer. 2014. Strontium isotope stratigraphy of the Gabbs Formation (Nevada): implications for global Norian–Rhaetian correlations and faunal turnover. *Lethaia* 47:500–511.

Tanner, L. H., S. G. Lucas, and M. G. Chapman. 2004. Assessing the record and causes of Late Triassic extinctions. *Earth-Science Reviews* 65:103–139.

Taylor, D., J. Guex, and S. G. Lucas. 2021. Ammonoids of the latest Triassic Gabbs Formation at New York Canyon, Mineral County, Nevada. *Fossil Record* 7:393–425.

Tipper, H. W., E. S. Carter, M. J. Orchard, and E. T. Tozer. 1994. The Triassic–Jurassic boundary in Queen Charlotte Islands, British Columbia defined by ammonites, conodonts and radiolarians. *Geobios Mémoire Special* 17:485–492.

Ward, P. D., J. W. Haggart, E. S. Carter, D. Wilbur, H. W. Tipper, and T. Evans. 2001. Sudden productivity collapse associated with the Triassic–Jurassic boundary mass extinction. *Science* 292:1148–1151.

Ward, P. D., G. H. Garrison, J. W. Haggart, D. A. Kring, and M. J. Beattie. 2004. Isotopic evidence bearing on Late Triassic extinction events, Queen Charlotte Islands, British Columbia, and implications for the duration and cause of the Triassic/Jurassic mass extinction. *Earth and Planetary Science Letters* 224:589–600.

Wignall, P. B., J. P. Zonneveld, R. J. Newton, K. Amor, M. A. Sephton, and S. Hartley. 2007. The end Triassic mass extinction record of Williston Lake, British Columbia. *Palaeogeography, Palaeoclimatology, Palaeoecology* 253:385–406.

Williford, K. H., P. D. Ward, G. H. Garrison, and R. Buick. 2007. An extended organic carbon-isotope record across the Triassic–Jurassic boundary in the Queen Charlotte Islands, British Columbia, Canada. *Palaeogeography, Palaeoclimatology, Palaeoecology* 244:290–296.

Williford, K. H., J. Foriel, P. D. Ward, and E. J. Steig. 2009. Major perturbation in sulfur cycling at the Triassic–Jurassic boundary. *Geology* 37:835–838.

Yager, J. A., A. J. West, F. A. Corsetti, W. M. Berelson, N. E. Rollins, S. Rosas, and D. J. Bottjer. 2017. Duration of and decoupling between carbon isotope excursions during the end-Triassic mass extinction and Central Atlantic Magmatic Province emplacement. *Earth and Planetary Science Letters* 473:227–236.

Zaffani, M., C. Agnini, G. Concheri, L. Godfrey, M. Katz, M. Maron, and M. Rigo. 2017. The Norian "chaotic carbon interval": new clues from the $\delta^{13}C_{org}$ record of the Lagonegro Basin (southern Italy). *Geosphere* 13:1–16.

Zhang, M., H. Jiang, M. A. Purnell, and X. Lai. 2017. Testing hypotheses of element loss and instability in the apparatus composition of complex conodonts: articulated skeletons of *Hindeodus*. *Palaeontology* 60:595–608.

Zimmerman, A. N., C. C. Johnson, and P. D. Polly. 2018. Taxonomic and evolutionary pattern revisions resulting from geometric morphometric analysis of Pennsylvanian *Neognathodus* conodonts, Illinois Basin. *Paleobiology* 44:660–683.